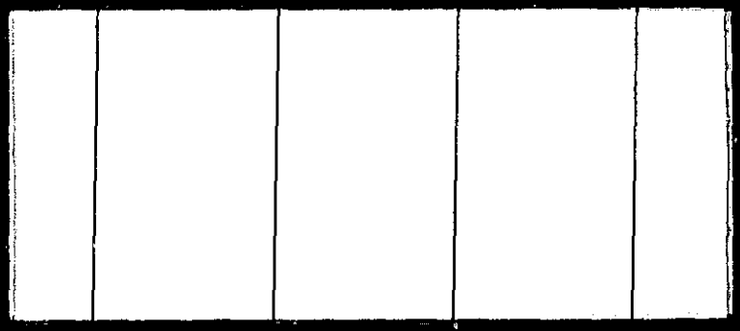

THE INVESTIGATION OF O AND N_2 DENSITIES FROM THE OSO-7 EXTREME UV DATA

FINAL REPORT

Submitted To: NASA
Code PY
Headquarters
Washington, D.C.

Submitted By: Wolf Research and Development Group
6801 Kenilworth Avenue
Riverdale, Maryland 20840

Date Submitted: February 3, 1975

Reference: WOLF No. 00079

TABLE OF CONTENTS

SUMMARY

This report presents the results of a study of solar radiation observations in the extreme ultra violet spectrum from 200 to 600 Å made by the OSO-7 satellite. The results of special interest in this work were those made under the influence of attenuation by the atmosphere in the 250 to 500 km. altitude range.

Using published molecular absorption cross-sections at 304 Å and 256 Å, we were able to validate the Jacchia atmospheric model (1971) and showed that a mean exospheric of 1050°K was appropriate for the sunset data. The cross-sections obtained by Hinteregger and Hall (1969) were shown to be most appropriate at 256 Å, whereas those of Knight, Uribe and Woodgate (1973) were employed for 304 Å. Employing the validated atmospheric model we were then able to derive values of 6.3 ± 0.6 Barns and 6.9 ± 3.0 Barns for the cross-sections of O and N_2, respectively at 285 Å and 7.6 ± 0.8 Barns and 4.8 ± 3.9 Barns for the respective cross-sections at 355 Å.

SECTION 1.0
INTRODUCTION

Wolf Research and Development Corporation is pleased to submit this final report on project NAS W-2595 to NASA Headquarters. The report describes the final results obtained in analyzing OSO-7 data to evaluate atmospheric absorption cross-sections in 300-500 km. altitude range and the 200-400 Å wavelength range.

All the analysis and results pertinent to the conclusions are presented in this report. In Section 2.0 the basic intensity analysis is given, followed by the geometrical and orbital analysis in Section 3.0. Section 4.0 gives a discussion of the results analysis and conclusions are presented in Section 5.0.

SECTION 2.0
ANALYSIS DESCRIPTION

The OSO-7 experimental tapes contain information on the date of acquisition of solar intensity data, orbital characteristic information and the observed intensities at one or two lines in the spectrum. The experimental data files are organized into pages or frames, there being 96 intensities collected over 15.36 seconds for each line being studied presented within each frame. The fundamental sampling interval was 160 milliseconds and the data appeared as photon counts.

For the purposes of our analysis the section of the quantity of data to average before applying an inversion analysis is indicated by the requirement for a suitable compromise between minimizing random errors and systematic errors. The greater the averaging time, the smaller the random error, but the larger the systematic error introduced by non-linearities in the model. In the work reported here we assumed that the average intensity at the midtime of a 5 second data span is sufficient. Thus we have averaged the intensity for three sections, each 32 points long, within each of the frames and printed out as shown in Figure 2.1. In the Figure 2.1, the various columns are as follows:

Frame: Experimental Frame Number

Midtime: Middle time of the experimental frame (seconds from start of day, Universal Time).

AVEUV1: Average intensity in the medium wavelength of the frame.

AVEUV2: Average intensity in the long wavelength of the frame.

FRAME	MIDTIME	AVEUV1	AVEUV2	X	Y	Z	ALTITUDE	SUN ANGLE
1	31036.659	5.196	2.683	-0.3145028146D 04	-0.4767032263D 04	-0.3640466719D 04	0.4012653838D 03	-0.2406122379D 00
2	31072.219	2.885	3.302	-0.3043358715D 04	-0.4829324364D 04	-0.3652461600D 04	0.4009976077D 03	-0.2238773939D 00
3	31087.573	7.760	6.208	-0.2940764553D 04	-0.4884344353D 04	-0.3663346006D 04	0.4049259464D 03	-0.2070834815D 00
4	31102.938	17.354	10.708	-0.2837277097D 04	-0.4933939955D 04	-0.3673116559D 04	0.4057481154D 03	-0.1902357354D 00
5	31119.297	27.792	16.729	-0.2738608703D 04	-0.4992205815D 04	-0.3681366159D 04	0.4086317792D 03	-0.1742491889D 00
6	31133.656	37.313	21.385	-0.2633494085D 04	-0.5043416602D 04	-0.3688977367D 04	0.4104804217D 03	-0.1573128576D 00
7	31149.016	45.917	25.406	-0.2527581615D 04	-0.5099647247D 04	-0.3695469983D 04	0.4123216399D 03	-0.1403381577D 00
8	31164.379	54.771	27.583	-0.2420887647D 04	-0.5147319465D 04	-0.3700843226D 04	0.4141535988D 03	-0.1237599844D 00
9	31179.738	56.667	30.417	-0.2313516699D 04	-0.5193746933D 04	-0.3705139929D 04	0.4161916445D 03	-0.1062858362D 00
10	31195.098	63.073	33.167	-0.2205426755D 04	-0.5242715010D 04	-0.3708287255D 04	0.4180524281D 03	-0.8922824608D-01
11	31210.457	67.510	34.458	-0.2096670883D 04	-0.5283100104D 04	-0.3710313682D 04	0.4199030537D 03	-0.7215319360D-01
12	31225.816	69.635	35.698	-0.1987828260D 04	-0.5331835340D 04	-0.3711218574D 04	0.4217412106D 03	-0.5506564408D-01
13	31241.176	69.302	36.021	-0.1877331616D 04	-0.5374302178D 04	-0.3711052440D 04	0.4237952291D 03	-0.3796670074D-01
14	31256.539	67.479	36.833	-0.1766767199D 04	-0.5414105656D 04	-0.3709735724D 04	0.4256706259D 03	-0.2086364400D-01
15	31271.898	65.104	36.127	-0.1655699234D 04	-0.5453376659D 04	-0.3707301476D 04	0.4275110109D 03	-0.3774629816D-02
16	31287.258	63.479	35.781	-0.1544133460D 04	-0.5491191104D 04	-0.3703750227D 04	0.4293472224D 03	0.1350922995D-01
17	31302.617	61.250	34.594	-0.1432124790D 04	-0.5527122545D 04	-0.3699136066D 04	0.4311406370D 03	0.3039535358D-01
18	31317.977	58.375	33.573	-0.1319679143D 04	-0.5561177357D 04	-0.3693375340D 04	0.4329655103D 03	0.4745270625D-01
19	31333.336	57.240	31.646	-0.1206837929D 04	-0.5593561130D 04	-0.3686509861D 04	0.4351090394D 03	0.6446219302D-01
20	31348.699	55.969	32.198	-0.1093606550D 04	-0.5624272944D 04	-0.3678532927D 04	0.4369356417D 03	0.8148728131D-01
21	31364.059	54.865	30.000	-0.9765506053D 03	-0.5654254021D 04	-0.3669177921D 04	0.4388891674D 03	0.9896551260D-01
22	31379.418	52.729	29.146	-0.8627290841D 03	-0.5681534271D 04	-0.3658370016D 04	0.4405918457D 03	0.1158910408D 00
23	31394.777	50.969	29.573	-0.7480445249D 03	-0.5707109123D 04	-0.3647664317D 04	0.4424719692D 03	0.1327726303D 00
24	31410.137	49.406	28.500	-0.6379007329D 03	-0.5733556579D 04	-0.3635750346D 04	0.4444760380D 03	0.1497760941D 00
25	31425.496	48.958	28.354	-0.5234162652D 03	-0.5752601581D 04	-0.3622316536D 04	0.4462564953D 03	0.1658555256D 00
26	31440.859	49.698	27.354	-0.4087480639D 03	-0.5773329385D 04	-0.3607795054D 04	0.4480181617D 03	0.1825809020D 00
27	31456.219	49.125	26.427	-0.2939894034D 03	-0.5792124014D 04	-0.3592197367D 04	0.4497527272D 03	0.1992385753D 00
28	31471.578	49.323	26.844	-0.1791386517D 03	-0.5809564255D 04	-0.3575658444D 04	0.4519211370D 03	0.2158318549D 00
29	31486.938	47.958	25.490	-0.6424433311D 02	-0.5825002454D 04	-0.3557949578D 04	0.4536785926D 03	0.2323479355D 00
30	31502.297	48.656	25.490	0.5066376005D 02	-0.5839677307D 04	-0.3539179439D 04	0.4554096665D 03	0.2487864629D 00
31	31517.656	48.948	24.938	0.1655591362D 03	-0.5850115856D 04	-0.3519356240D 04	0.4571121145D 03	0.2651427410D 00
32	31533.016	47.698	23.938	0.2804436717D 03	-0.5861247666D 04	-0.3498607931D 04	0.4592530828D 03	0.2814162496D 00
33	31548.379	47.135	24.063	0.3952317083D 03	-0.5869744790D 04	-0.3476716543D 04	0.4609756650D 03	0.2975974429D 00
34	31563.738	46.625	23.844	0.5098709911D 03	-0.5876937630D 04	-0.3453797071D 04	0.4625696091D 03	0.3136784151D 00
35	31579.098	47.771	22.931	0.6243557621D 03	-0.5881494946D 04	-0.3429850983D 04	0.4643313312D 03	0.3296587594D 00
36	31594.457	46.063	21.281	0.7387326735D 03	-0.5885215164D 04	-0.3405008098D 04	0.4664368209D 03	0.3455387013D 00
37	31609.816	47.333	21.823	0.8528174599D 03	-0.5886792719D 04	-0.3379062431D 04	0.4681168236D 03	0.3613036827D 00
38	31625.176	46.823	20.740	0.9666472167D 03	-0.5886325333D 04	-0.3352115686D 04	0.4697669896D 03	0.3769547087D 00
39	31640.539	45.927	21.094	0.1080216360D 04	-0.5884712285D 04	-0.3324168731D 04	0.4713855565D 03	0.3924913604D 00
40	31655.898	44.719	19.813	0.1193550714D 04	-0.5881187609D 04	-0.3295357089D 04	0.4734425516D 03	0.4079066866D 00
41	31671.258	44.365	20.563	0.1306428284D 04	-0.5875193645D 04	-0.3265486627D 04	0.4750738286D 03	0.4231892796D 00
42	31686.617	44.760	19.208	0.1418917616D 04	-0.5868132561D 04	-0.3234652007D 04	0.4766739227D 03	0.4383407977D 00
43	31701.977	44.313	20.104	0.1530984830D 04	-0.5860337556D 04	-0.3202862474D 04	0.4782406262D 03	0.4533570804D 00
44	31717.336	43.104	19.167	0.1642749126D 04	-0.5850264282D 04	-0.3170228375D 04	0.4802415336D 03	0.4682397815D 00
45	31732.699	44.802	18.635	0.1753923867D 04	-0.5838080196D 04	-0.3136577086D 04	0.4818185712D 03	0.4829765318D 00
46	31748.059	44.093	18.719	0.1864551499D 04	-0.5824180004D 04	-0.3102011243D 04	0.4833626673D 03	0.4975621199D 00
47	31763.418	42.927	18.385	0.1974627097D 04	-0.5808364922D 04	-0.3066332749D 04	0.4848372774D 03	0.5119963564D 00
48	31778.777	43.740	17.927	0.2084303825D 04	-0.5791570637D 04	-0.3030238773D 04	0.4868284625D 03	0.5262815456D 00
49	31794.137	43.948	17.688	0.2193206184D 04	-0.5772717414D 04	-0.2992992493D 04	0.4883246009D 03	0.5404010106D 00
50	31809.496	43.655	18.333	0.2301462758D 04	-0.5752063999D 04	-0.2954868393D 04	0.4898071394D 03	0.5543576037D 00
51	31824.859	43.646	18.365	0.2409066069D 04	-0.5729716602D 04	-0.2915867825D 04	0.4912544765D 03	0.5681510727D 00
52	31840.219	44.156	17.740	0.2516150856D 04	-0.5706109314D 04	-0.2875992722D 04	0.4931176514D 03	0.5817772636D 00
53	31855.578	43.917	18.010	0.2622710175D 04	-0.5681479293D 04	-0.2835426906D 04	0.4945678868D 03	0.5952226664D 00
54	31870.938	43.948	18.073	0.2727699855D 04	-0.5655187782D 04	-0.2794932196D 04	0.4959836445D 03	0.6084906101D 00
55	31886.297	44.104	17.250	0.2832188384D 04	-0.5628242553D 04	-0.2753620946D 04	0.4973630946D 03	0.6215778534D 00
56	31901.656	44.271	17.833	0.2936286111D 04	-0.5599941977D 04	-0.2709558764D 04	0.4991452021D 03	0.6344869253D 00
57	31917.016	44.948	17.917	0.3039218150D 04	-0.5569379817D 04	-0.2664672155D 04	0.5005244951D 03	0.6472014190D 00
58	31932.379	44.354	18.563	0.3141287102D 04	-0.5537060461D 04	-0.2619997610D 04	0.5018599516D 03	0.6597279531D 00
59	31947.738	44.042	19.438	0.3242416622D 04	-0.5503603997D 04	-0.2574571113D 04	0.5031760857D 03	0.6720568809D 00
60	31963.098	43.875	18.906	0.3342847533D 04	-0.5469150092D 04	-0.2528429536D 04	0.5048698117D 03	0.6841951179D 00
61	31979.457	43.688	18.094	0.3442095120D 04	-0.5417321653D 04	-0.2481533871D 04	0.5061734501D 03	0.6961255089D 00

FIGURE 2.1. COMPUTER OUTPUT SHOWING AVERAGED INTENSITY AND ORBITAL DATA

X, Y, Z: Satellite geocentric coordinates in km. at the midtime of the experimental frame.

Altitude: Altitude of the satellite from the Earth's surface in km. at the midtime of the experimental frame.

Sun Angle: Cosine of the angle between the lines joining the satellite and solar center to the geocenter.

The calculation of the position, altitude and the Sun angle of the satellite will be discussed in detail in Section 3.0.

The intensity data at a given wavelength λ is measured by the satellite instrument. We assumed that when the path from the satellite to the Sun did not pass through any layer below 480 kms. there was no significant attenuation. Thus this data was accumulated and averaged to give the mean intensity per observation for zero attenuation, $I_{0\lambda}$.

When the path from the satellite to the Sun fell below 480 kms. the mean intensity per observation I_λ generally fell below $I_{0\lambda}$ indicating attenuation. The total optical thickness along the path through the atmosphere could be estimated as:

$$\tau_\lambda = \log_e \left(\frac{I_{0\lambda}}{I_\lambda} \right) \qquad (2.1)$$

When the Sun-satellite line fell below the 300 km. altitude it was found that no significant signal was received. Thus the intensity yields information about attenuation in the 260 to 480 km. altitude range.

We divided the atmosphere in this altitude range into 22 layers each 10 kms. thick. This was considered to be the greatest degree of detail we could reasonably consider when using one file of data (one orbit) only.

The equation used for analyzing the data was

$$\tau_{\lambda j} = \sum_i F_{ij}\, \sigma_{i\lambda} \qquad (2.2)$$

where

$\tau_{\lambda j}$ is the j^{th} observation of optical thickness at wavelength λ.

F_{ij} is the path length in kms. through the i^{th} layer for the j^{th} observation (see next section).

$\sigma_{i\lambda}$ is the mean absorption cross-section in the i^{th} layer (km^{-1}).

$\sigma_{i\lambda}$ is made up of two parts, one for absorption by 0 and the other for absorption by N_2. If (n_{0i}, n_{Ni}) are the mean densities of 0 and N_2, respectively in the i^{th} layer and $\sigma_{0\lambda}$ and $\sigma_{N\lambda}$ are the respective cross-sections at wavelength λ we have that

$$\sigma_{i\lambda} = n_{0i}\, \sigma_{0\lambda} + n_{Ni}\, \sigma_{N\lambda} \qquad (2.3)$$

Thus the values of λ_i contain information about both the O and N_2 densities, as well as their cross-sections. Clearly, we need to know at least 3 of the 4 unknowns in each layer before the other parameter can be determined. Therefore, even if the cross-sections are known it is impossible to unambiguously derive both the N_2 and O densities independently.

The procedure we employed in our analysis was to use the standard atmospheres of Jacchia (1971) to determine the appropriate range of exospheric temperatures where the cross-sections were known (256 Å and 304 Å) and then to employ a least squares analysis to derive the cross-sections $\sigma_{N\lambda}$ and $\sigma_{0\lambda}$ at the wavelengths where they were not known (285 Å and 355 Å). The details of the results will be considered in Section 4.0 of this report.

In deriving the values of $\sigma_{i\lambda}$ using equations of the form of (2.2), it was necessary to determine the appropriate weighting factor to be used with each equation. The objective was to evaluate the variance, σ^2, in τ_λ and then divide the corresponding equation by σ.

Suppose that $I_{0\lambda}$ was derived from a total of $N_{0\lambda}$ counts over a time $T_{0\lambda}$ and I_λ was derived from a total of N_λ counts over a time T_λ. Then

$$\left.\begin{aligned} I_{0\lambda} &= N_{0\lambda}\ T_{0\lambda}^{-1} \\ I_\lambda &= N_\lambda\ T_\lambda^{-1} \end{aligned}\right\} \qquad (2.4)$$

Then

$$\left.\begin{aligned} V(I_{0\lambda}) &= N_{0\lambda}\ T_{0\lambda}^{-2} \\ V(I_{\lambda}) &= N_{\lambda}\ T_{\lambda}^{-2} \end{aligned}\right\} \tag{2.5}$$

give the variances in $I_{0\lambda}$ and I_{λ}, respectively, since $N_{0\lambda}$ and N_{λ} are Poisson counts.

It follows that

$$\left.\begin{aligned} I_{0\lambda}^{-2}V(I_{0\lambda}) &= N_{0\lambda}^{-1} \\ I_{\lambda}^{-2}V(I_{\lambda}) &= N_{\lambda}^{-1} \end{aligned}\right\} \tag{2.6}$$

and

$$V\left(\frac{I_{0\lambda}}{I_{\lambda}}\right) = \left(\frac{I_{0\lambda}}{I_{\lambda}}\right)^2\left(\frac{1}{N_{0\lambda}} + \frac{1}{N_{\lambda}}\right) \tag{2.7}$$

Using (2.1) we then obtain the simple result,

$$V(\tau_{\lambda}) = \left(\frac{1}{N_{0\lambda}} + \frac{1}{N_{\lambda}}\right) \tag{2.8}$$

which is the required variance, σ^2.

A series of experiments we performed on the inversion of overdetermined linear equations indicated that the best combination of accuracy and computer time requirement would be yielded by the IBM systems subroutines package inversion programs LLSQ and DLLSQ. In practical applications, however, these solution procedures failed to successfully invert (2.1) consistently. The reason for this failure is not clear but we believe it relates to the substantial random errors occurring in the τ_j estimates. The program was carefully checked to eliminate any possible dimensioning or other errors and the fact that the routine successfully inverted some data sets, supports the hypothesis that the routines were being employed correctly.

The lack of consistency in producing successful inversions seriously slowed our production analysis activity. As a consequence we developed a new procedure which has proved to be very stable and reliable, while producing sensible answers consistent with those generated by successful LLSQ runs. The procedure is based on the summation of sets of equations of the form (2.1) to generate a right upper triangular matrix on the left-hand side. This proved to be particularly easy to accomplish since the altitude of the grazing incidence increased monotonically during sunrise and decreased monotonically during sunset. (This altitude establishes the number of leading zero F_{ij} values in (2.1).) Thus the procedure required merely the summing of sets of adjacent model equations. Non-singularity was assured in all practical cases by the stipulation that there should be at least one grazing incidence in each layer of the atmospheric model. This is discussed more fully in Section 3.1.

Once the left-hand side matrix is right upper triangular, the cross-section in the top layer can be solved for immediately and successive back substitution employed

to sections within all other layers. In practice, we have found that the solution can be generated in much less time than by LLSQ since the procedure requires N^2 multiplications compared to $N^2(N+n)$ for the standard least squares procedure. (N is the number of coefficients and n the number of equations.) The results generated by the application of the new routine to the data analyzed in the previous report gave cross-section profiles very similar to those yielded in LLSQ.

SECTION 3.0
ORBITAL INTERPOLATION AND GEOMETRIC ANALYSIS

3.1 ORBITAL INTERPOLATION

The data tapes contain orbital data in geocentric coordinates at one minute intervals as illustrated in Figure 3.1 of the first quarterly progress report on this project. The problem that we considered was that of obtaining the geocentric coordinates at the mid points of the experimental frames using the given data at one minute intervals.

The first step was to compute the nearest given orbital data point to the frame mid point. Clearly this could not be more than 30 seconds away. We thus knew the orbital elements including velocity components at an epoch t and wished to compute the elements at a time $t + \Delta t$ where Δt was in the range -30 seconds to +30 seconds. Let $X_i(t)$ be the ith coordinate at time t. Cowell's equations for two body motion is

$$\ddot{X}_i = - \frac{X_i}{R^3} \qquad (3.1)$$

where μ is the gravitational constant = 3.986013×10^5 km^3 sec^{-2}

and R is the geocentric radius
$= (\Sigma_{i=1}^{3} X_i^2)^{1/2}$

In making the analysis we neglected the time variation of R since the OSO-7 orbit is not far from circular (eccentricity around 0.0165). Thus we obtained from equation (3.1)

TAPE NUMBER= CA0614 FILE NUMBER= 62
FRAME NUMBER= 103 YEAR= 1972 DAY OF YEAR= 66 TIME OF DAY= 36180 SECON DS

MEDIUM WAVELENGTH= 314.90 ANGSTROMS LONG WAVELENGTH= 368.10 ANGSTROMS

	X	Y	Z	
SATELLITE POSITION	-0.5065846967D 04	-0.2382566830 04	-0.27864268800 04	(KMS.)
SATELLITE VELOCITY	0.3846352428D 01	-0.3119421840D 01	-0.2795339048D 01	(KMS./SEC.)
SOLAR POSITION	0.9625659316D 00	-0.2211513139D 00	-0.9590211883D-01	(A.U)

TAPE NUMBER= CA0614 FILE NUMBER= 62
FRAME NUMBER= 104 YEAR= 1972 DAY OF YEAR= 66 TIME OF DAY= 36240 SECON DS

MEDIUM WAVELENGTH= 314.90 ANGSTROMS LONG WAVELENGTH= 368.10 ANGSTROMS

	X	Y	Z	
SATELLITE POSITION	-0.5401704529D 04	-0.2725514044D 04	-0.2947451874D 04	(KMS.)
SATELLITE VELOCITY	0.4280499935D 01	-0.3913403434D 01	-0.2869350094D 01	(KMS./SEC.)
SOLAR POSITION	0.9625689387D 00	-0.2211405183D 00	-0.9589749109D-01	(A.U)

TAPE NUMBER= CA0614 FILE NUMBER= 62
FRAME NUMBER= 105 YEAR= 1972 DAY OF YEAR= 66 TIME OF DAY= 36300 SECON DS

MEDIUM WAVELENGTH= 314.90 ANGSTROMS LONG WAVELENGTH= 368.10 ANGSTROMS

	X	Y	Z	
SATELLITE POSITION	-0.5132335754D 04	-0.3074142517D 04	-0.3094562836D 04	(KMS.)
SATELLITE VELOCITY	0.4693456623D 01	-0.3692049921D 01	-0.2331804663D 01	(KMS./SEC.)
SOLAR POSITION	0.9625720382D 00	-0.2211298477D 00	-0.9589286423D-01	(A.U)

TAPE NUMBER= CA0614 FILE NUMBER= 62
FRAME NUMBER= 106 YEAR= 1972 DAY OF YEAR= 66 TIME OF DAY= 36360 SECON DS

MEDIUM WAVELENGTH= 314.90 ANGSTROMS LONG WAVELENGTH= 368.10 ANGSTROMS

	X	Y	Z	
SATELLITE POSITION	-0.4836869566D 04	-0.3408233281D 04	-0.3227102448D 04	(KMS.)
SATELLITE VELOCITY	0.5083323419D 01	-0.3433601375D 01	-0.2083915591D 01	(KMS./SEC.)
SOLAR POSITION	0.9625751376D 00	-0.2211917733D 00	-0.9588837747D-01	(A.U)

TAPE NUMBER= CA0614 FILE NUMBER= 62
FRAME NUMBER= 107 YEAR= 1972 DAY OF YEAR= 66 TIME OF DAY= 36420 SECON DS

MEDIUM WAVELENGTH= 314.90 ANGSTROMS LONG WAVELENGTH= 368.10 ANGSTROMS

	X	Y	Z	
SATELLITE POSITION	-0.4522744629D 04	-0.3972637567D 04	-0.3344427366D 04	(KMS.)
SATELLITE VELOCITY	0.5448351622D 01	-0.3190418451D 01	-0.1826936021D 01	(KMS./SEC.)
SOLAR POSITION	0.9625762371D 00	-0.2211085074D 00	-0.9588360973D-01	(A.U)

FIGURE 3.1. COMPUTER OUTPUT OF ORBITAL DATA

$$\frac{d^i X_i}{dt^j} = -\frac{\mu}{R^3} \frac{d^{j-2} X_i}{dt^{j-2}} \qquad (3.2)$$

and then employed the truncated Taylor series

$$X_i(t+\Delta t) = X_i(t) + \Sigma_{j=1}^{N} \frac{1}{j!} \frac{d^j X_i}{dt^j}(t) \Delta t^j \qquad (3.3)$$

The computed elements were employed to evaluate the appropriate altitude and sun angle. In computing the altitude we allowed for the earth's flatness, f, using the relationship

$$R_E = R_0 \left(1-f(1 + 1.5f) \sin^2\phi \left(1 - \sin^2\phi/(1 + \frac{2}{3} f^2)\right)\right) \qquad (3.4)$$

where R_E is the distance from the geocenter to the earth's surface at latitude ϕ and R_0 is the equatorial radius. f was taken to be $\frac{1}{298.5}$. R_E changed by about 5 kms. over the orbit.

In Figure 3.2 we present the computed altitude as a function of time for three orders of interpolation (2, 3 and 4). (It should be pointed out that the lack of continuity seen in the N=2 data was the worst of any data analyzed to date.) On the basis of these data we have elected to use fourth order near circular orbit interpolation for all future runs.

The sun angle was computed using geocentric solar position coordinates obtained by linear interpolation between the one minute values extracted from the data tape. A plot of

FIGURE 3.2. OSO–7 ALTITUDE VS TIME FOR VARIOUS ORDERS OF INTERPOLATION

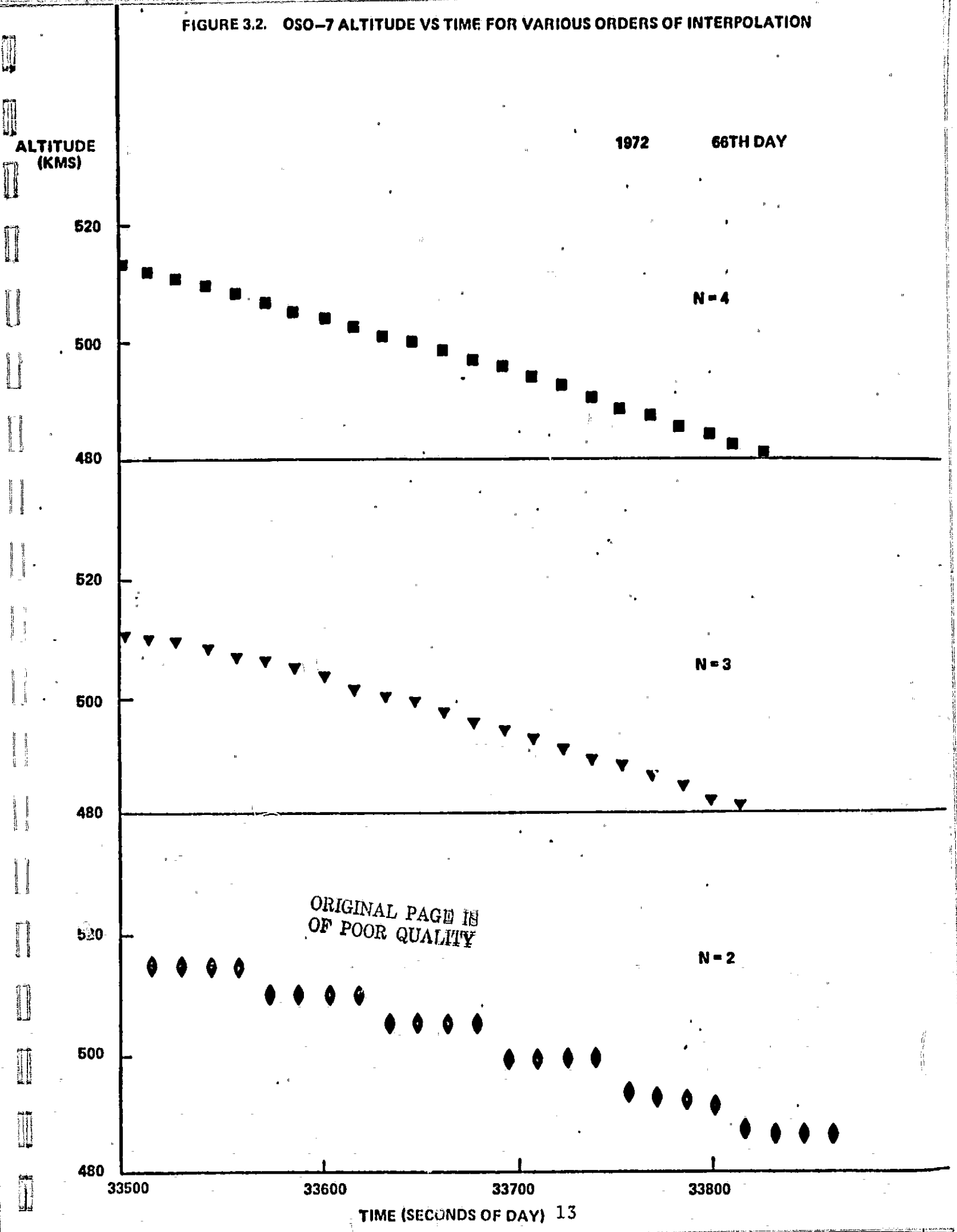

the geocentric solar position coordinates against time indicated that the errors arising from this procedure would be negligible.

3.2 GEOMETRIC ANALYSIS

In order to analyze the optical thickness data we needed to compute the distance covered through each atmospheric layer of our model. The philosophy employed here was that the earth was spherical, the radius being that appropriate for the latitude of the satellite at the time of data acquisition. This was assumed to give a reasonable representation of the atmospheric layer structure while reducing the computer time for the analysis to a minimum.

Figure 3.3 presents the geometry of the problem in the plane of the geocenter, the satellite and the Sun. P represents the satellite, the solar angle, ϕ, of the satellite being as shown. On the path to the Sun from P, A is the point of closest approach, distant R sin ϕ from the geocenter, where, R is the geocentric radius to the satellite. Using Pythagorus's theorem the distance covered between the Jth and (J+1) the layer <u>beneath</u> the satellite altitude is

$$2\left[\sqrt{R_{J+1}^2 - R^2 \sin^2\phi} - \sqrt{R_J^2 - R^2 \sin^2\phi}\right]$$

whereas the corresponding value for layers above the satellite altitude is the same, but with the 2 replaced by unity. R_J is the geocentric radius of the Jth atmospheric layer.

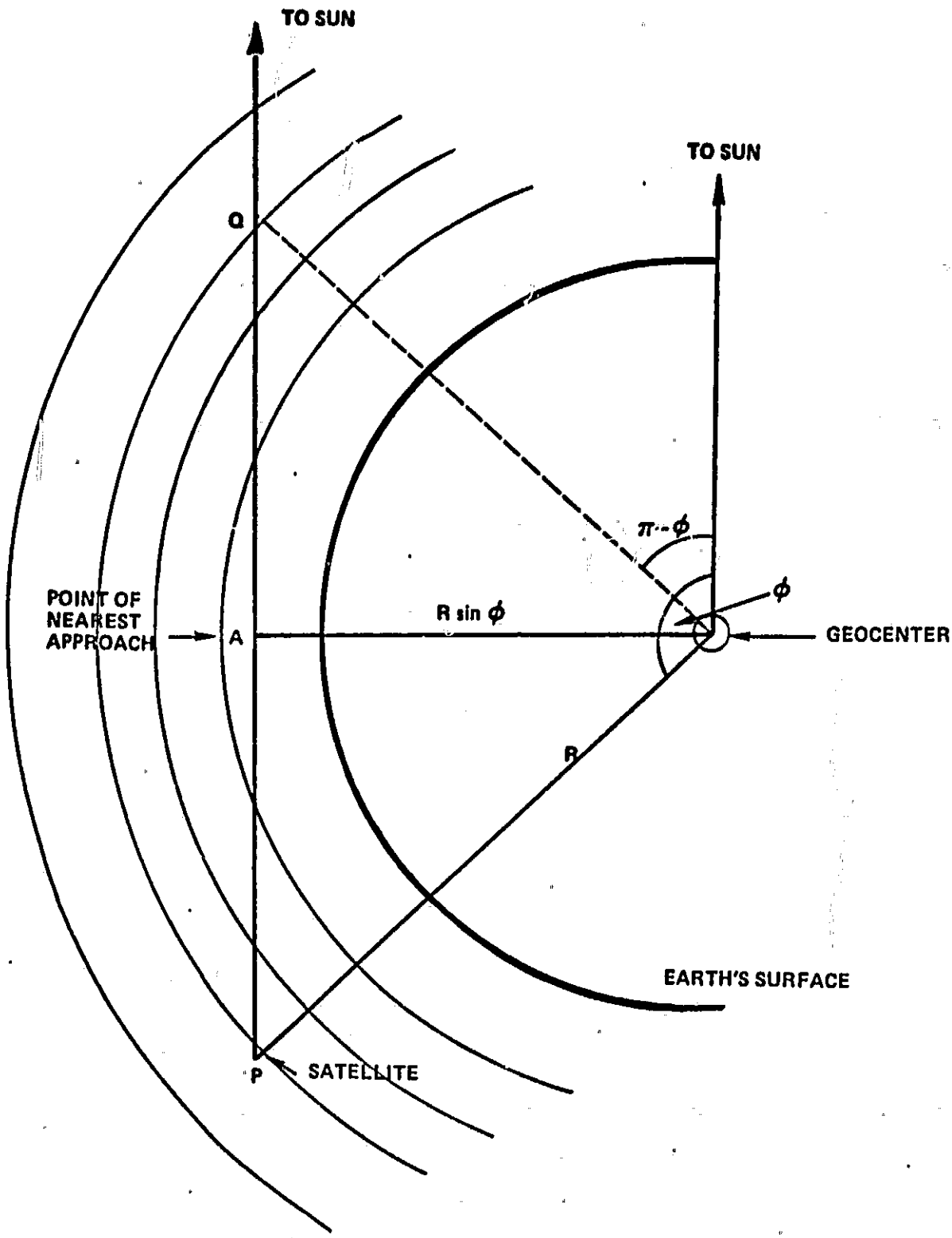

FIGURE 3.3. GEOMETRIC ANALYSIS

Clearly, if R sin ϕ is less than R_E+h_{min} where R_E is the (local) earth radius and h_{min} the lowest altitude considered and ϕ is greater than $\frac{\pi}{2}$ then no signal can be received, and the data point is ignored.

Suppose that R_K is the radius of the lowest layer boundary crossed by the path. In this case, the distance covered by the path in the Kth layer is just

$$2\sqrt{R_K^2 - R^2 \sin^2\phi}$$

If P is in the m th layer then the total distance covered in this layer in the case shown is

$$\sqrt{R_m^2 - R^2 \sin^2\phi} \cdot 2\sqrt{R_{m-1}^2 - R^2 \sin^2\phi} - R\cos\phi$$

The formulae given here were sufficient to evaluate the distance parameters F_{ij} of equation 2.2.

SECTION 4.0
RESULTS OF THE ANALYSIS

The cross-sections per km. were calculated from the data in each layer of the atmosphere from 260 km. to 480 km. The thickness of each layer was 10 km. The total cross-sections from each file for the wavelength of interest are plotted. These are shown in Figures 4.1 to 4.8.

We have fitted the data for 304 and 256 Å models with different exospheric temperatures. The three solid curves shown in the Figures 4.1 to 4.4 are from these models and we see that exospheric temperature 1050° models fits well with the data at sunset at 304 and 256 Å. The total cross-sections obtained from Jacchia models used Knight et al (1973) 256 Å and Hinteregger and Hall (1969) 304 Å absolute cross-sections. We see that the data at lower level layers at sunrise is consistent with sunset data; however, at higher altitudes the sunrise data has large scatter. This scatter possibly can be attributed to some interlocking problems and possibly atmospheric instabilities while heating. Due to lack of knowledge of the cross-sections as a function of temperature and the temperature change itself at the different altitudes, we elected at present to look at the sunset data only.

We derived our estimates of nitrogen and oxygen densities from the best fitted Jacchia model and presented in Table I for 304 and 256 Å. Using these densities in turn at 285 Å and 355 Å, we derived the absolute cross-sections of oxygen and nitrogen at these wavelengths as shown in Section 2.0. The cross-sections thus derived are given in Table II. These cross-sections are new in literature as far as we know. We thus have the densities N_2 and O and cross-sections at 285 Å and 355 Å.

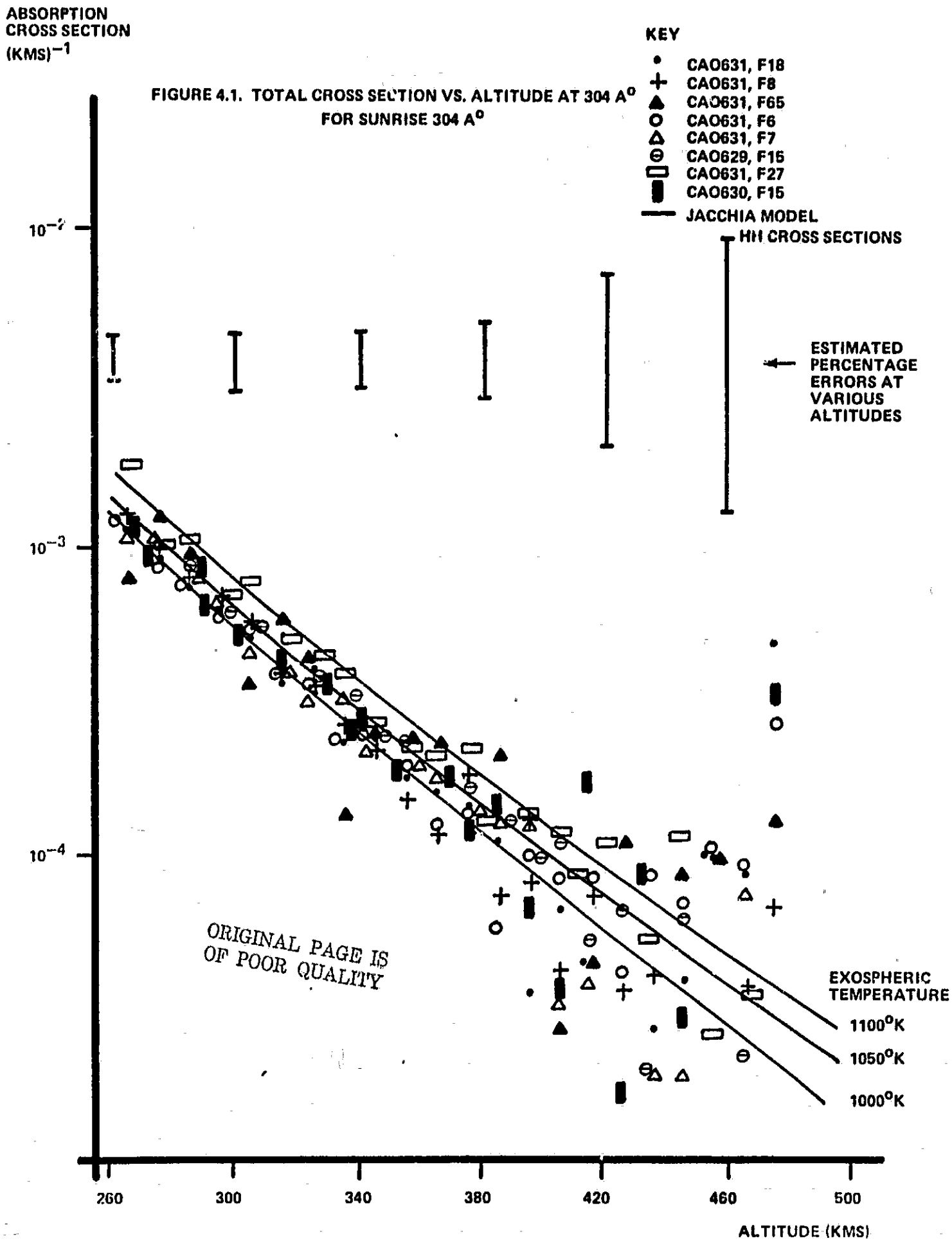

FIGURE 4.1. TOTAL CROSS SECTION VS. ALTITUDE AT 304 A° FOR SUNRISE 304 A°

FIGURE 4.2. TOTAL CROSS SECTION VS. ALTITUDE AT 256 A°
FOR SUNSET 256 A°

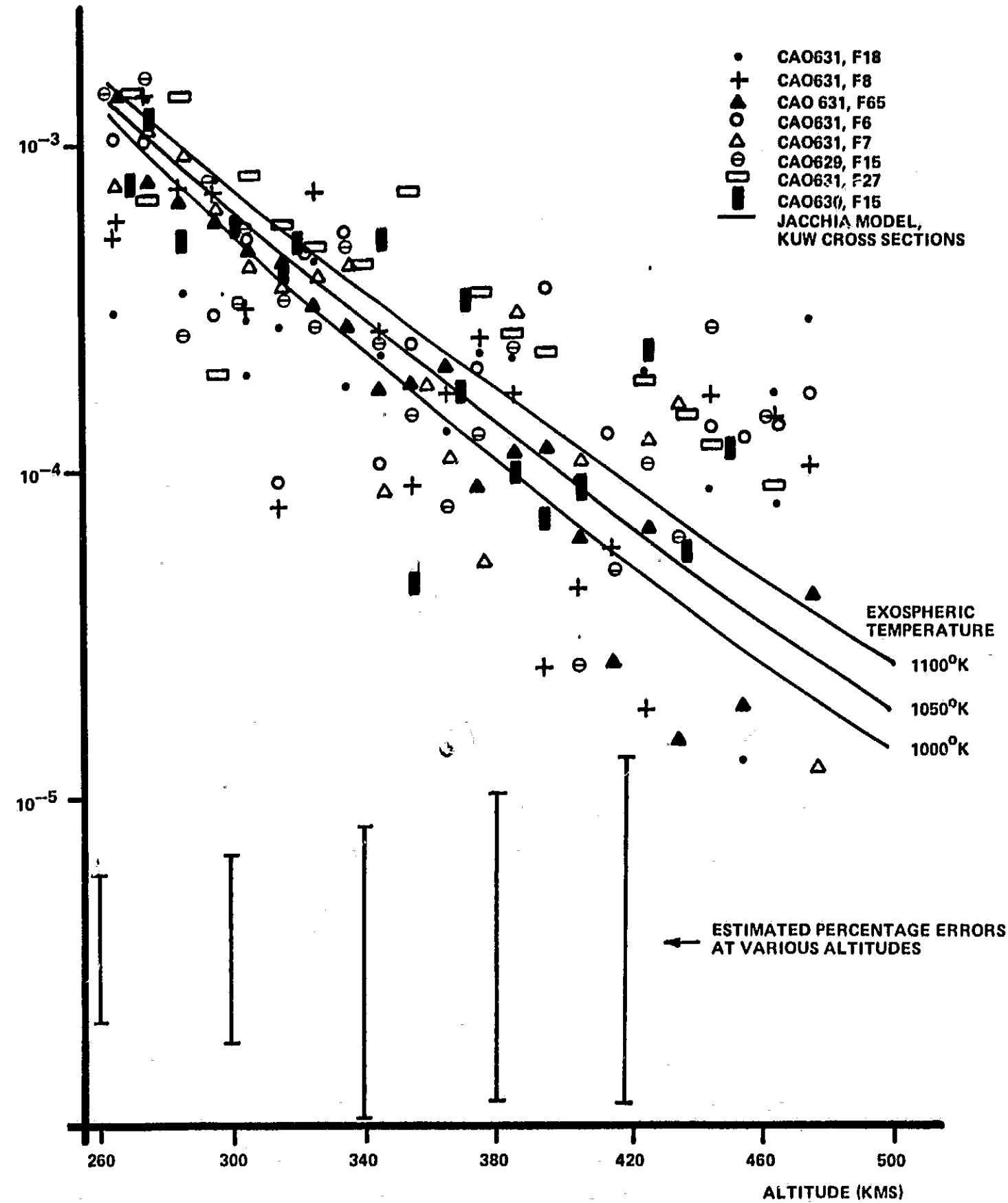

FIGURE 4.3. TOTAL CROSS SECTION VS. ALTITUDE AT 304 A^{o}
FOR SUNRISE 304 A^{o}

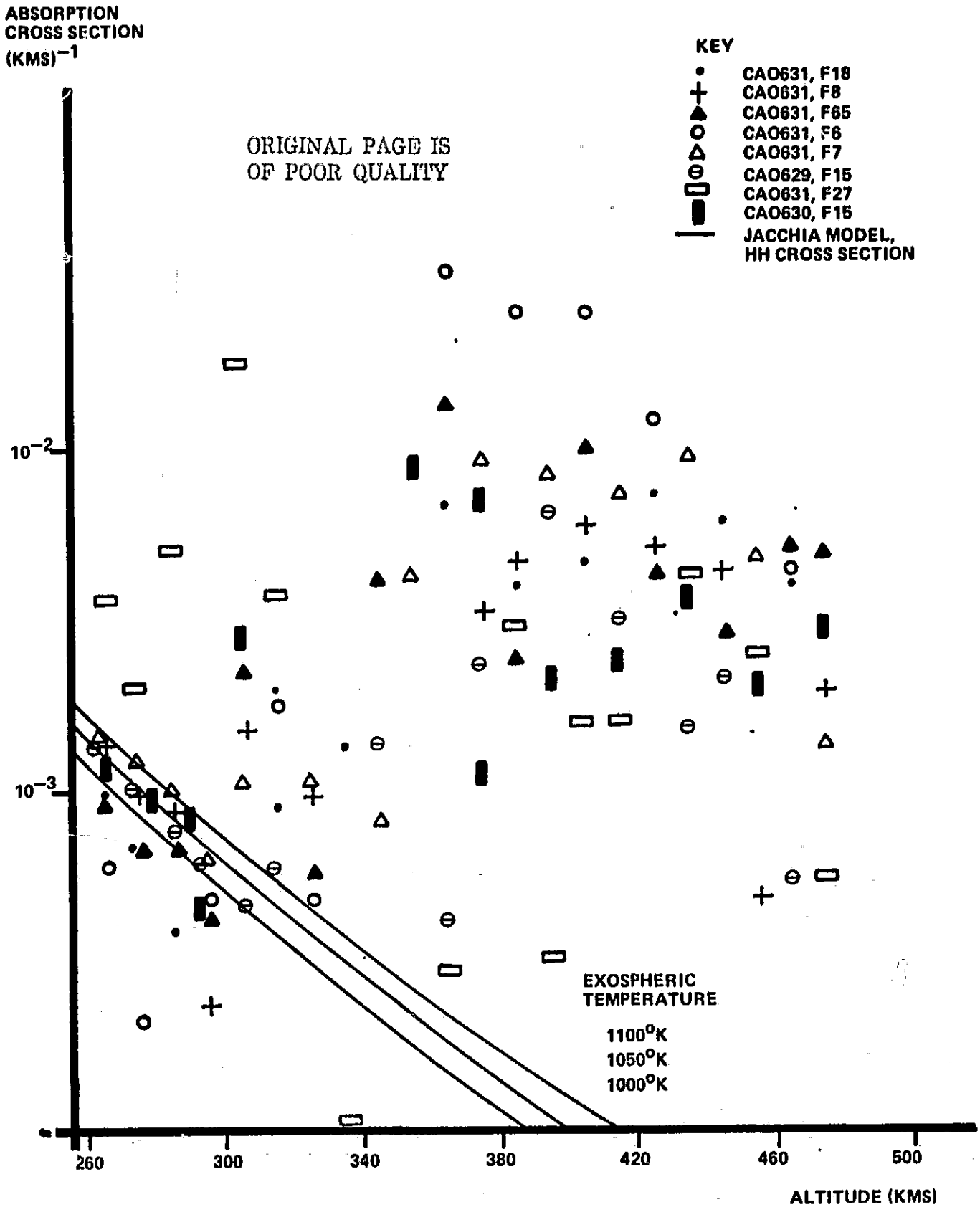

FIGURE 4.4. TOTAL CROSS SECTION VS. ALTITUDE AT 256 A^{o}
FOR SUNRISE 256 A^{o}

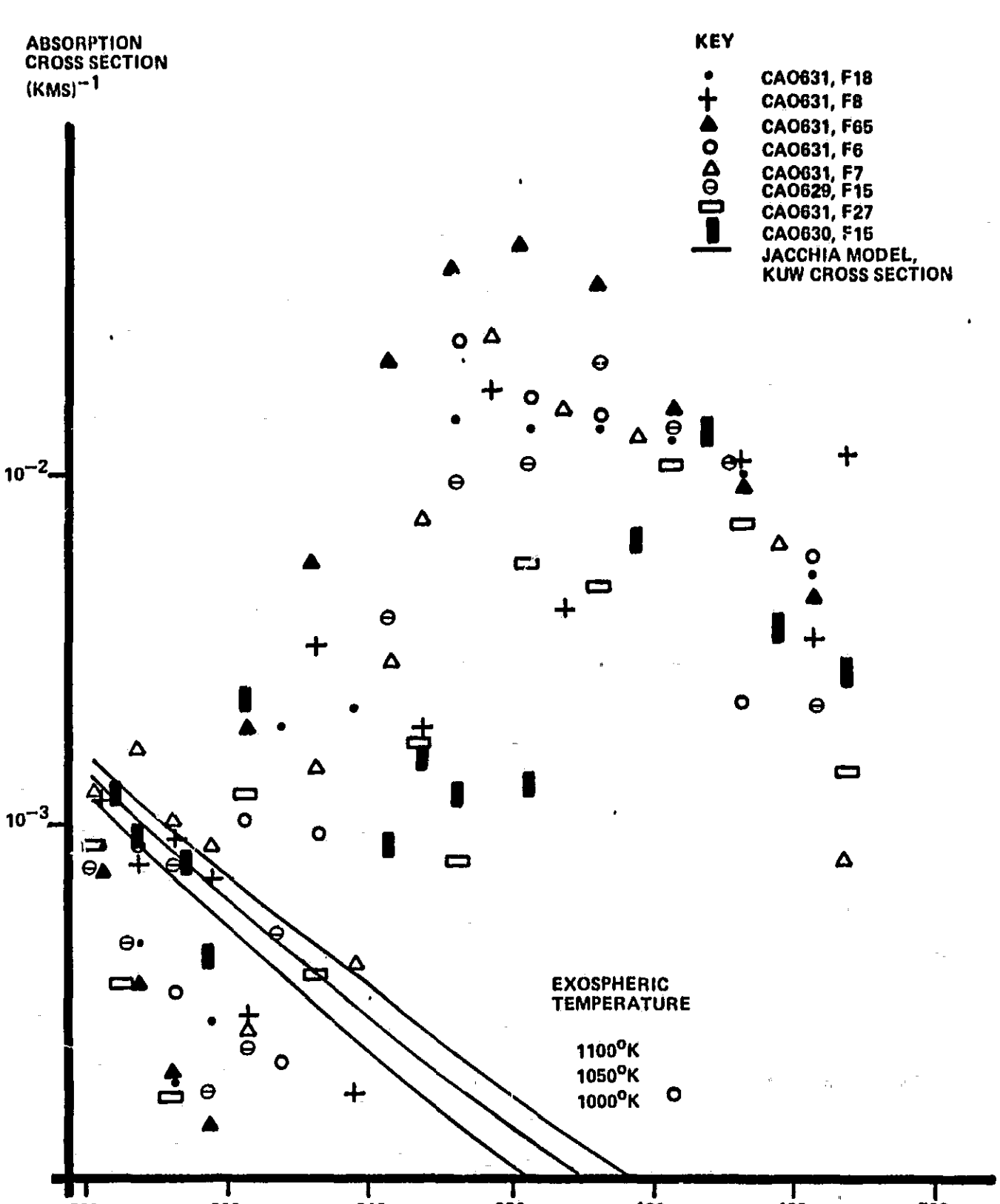

FIGURE 4.5. TOTAL CROSS SECTION VS. ALTITUDE AT 285 A°
FOR SUNSET 285 A°

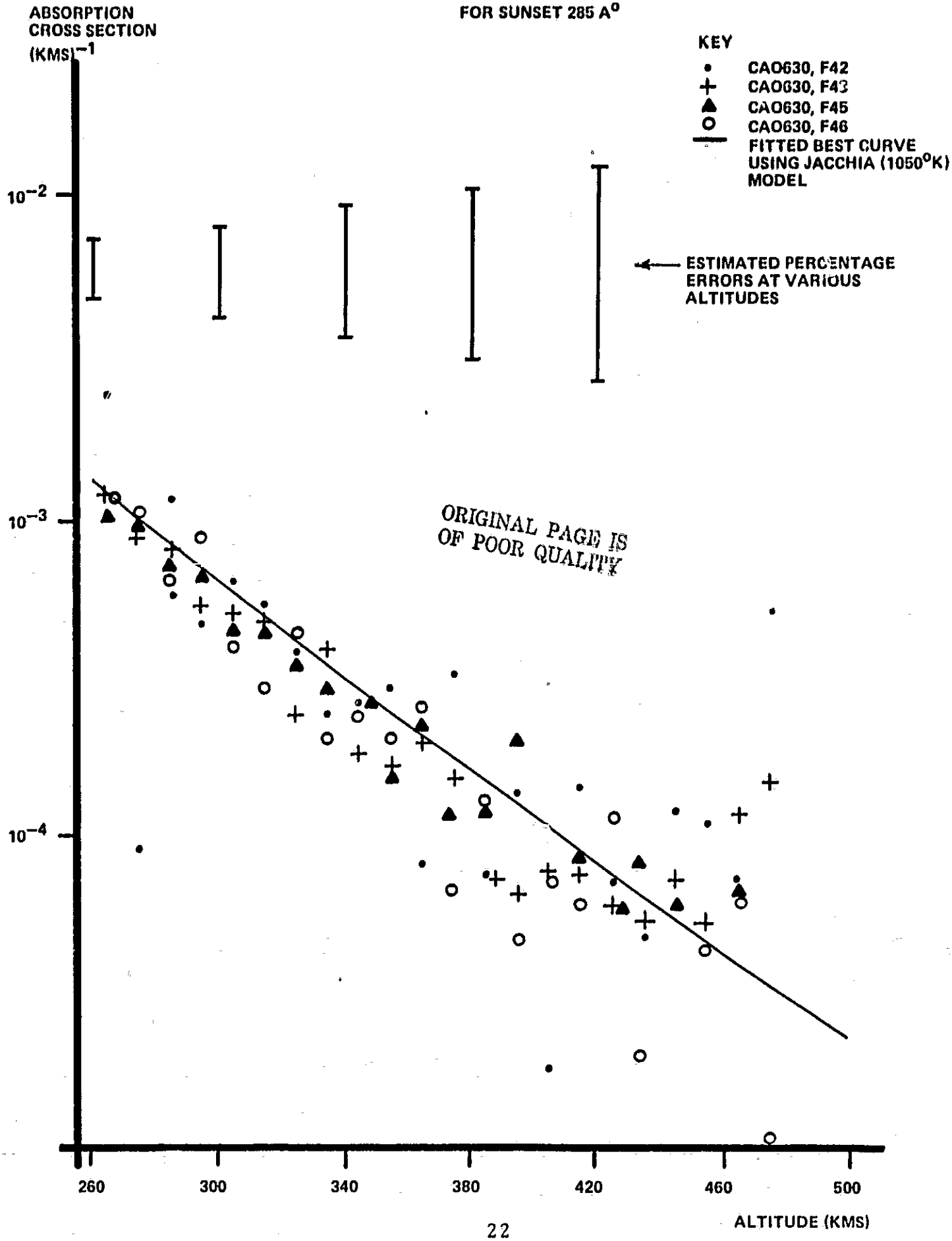

FIGURE 4.6. TOTAL CROSS SECTION VS. ALTITUDE AT 355 A°
FOR SUNSET 355 A°

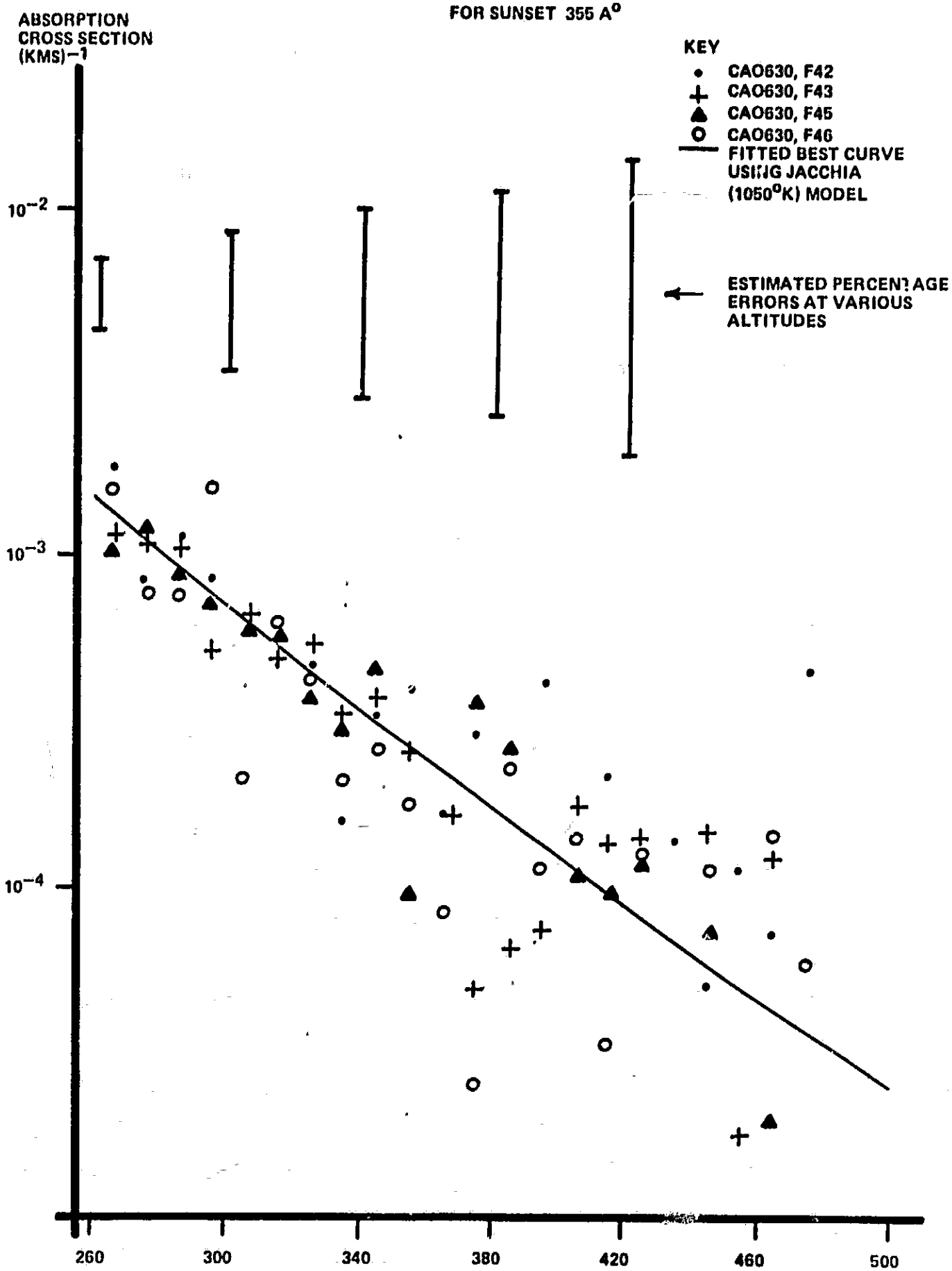

FIGURE 4.7. TOTAL CROSS SECTION VS. ALTITUDE AT 285 A°

FOR SUNRISE 285 A°

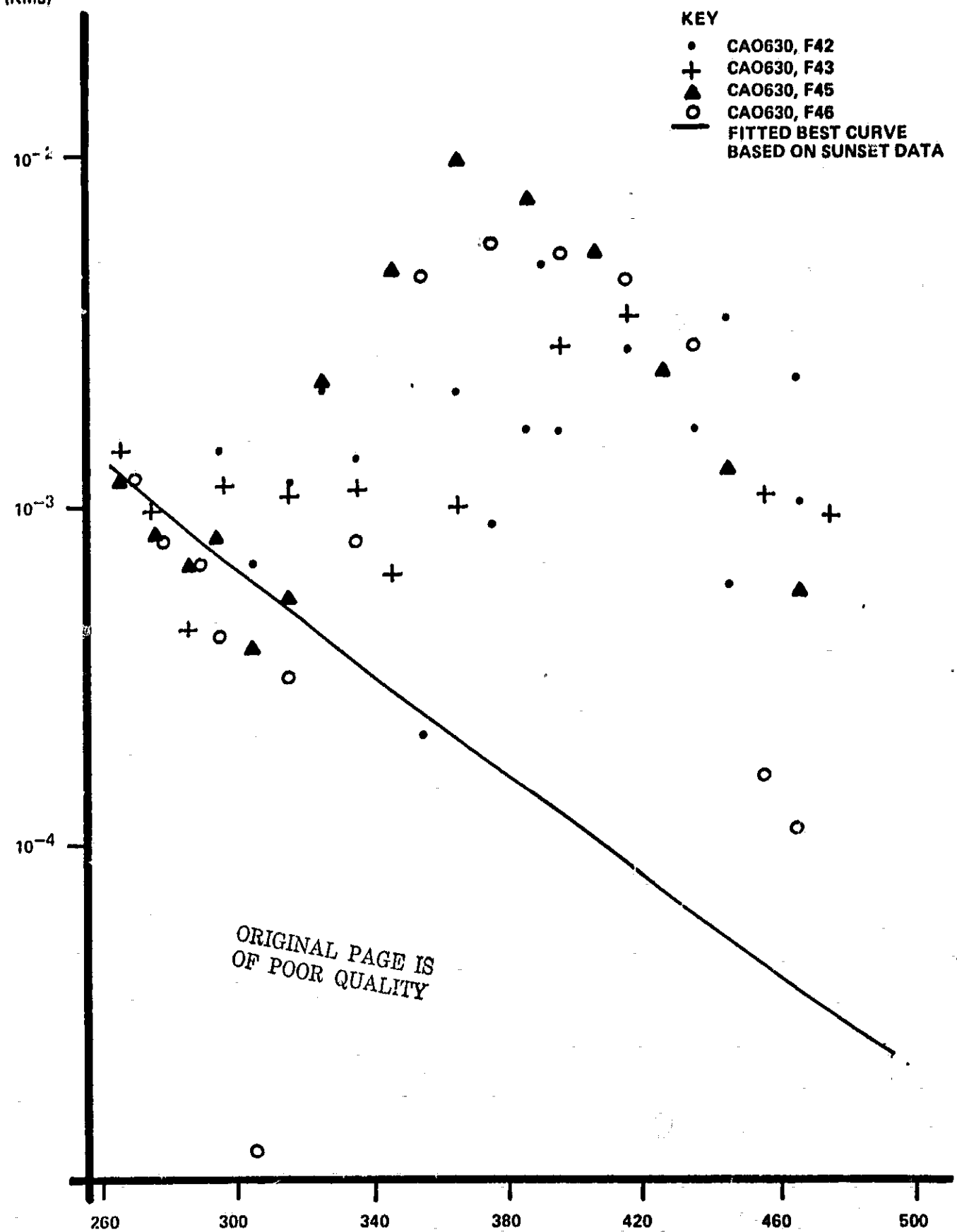

FIGURE 4.8. TOTAL CROSS SECTION VS. ALTITUDE AT 355 A^{o} FOR SUNRISE 355 A^{o}

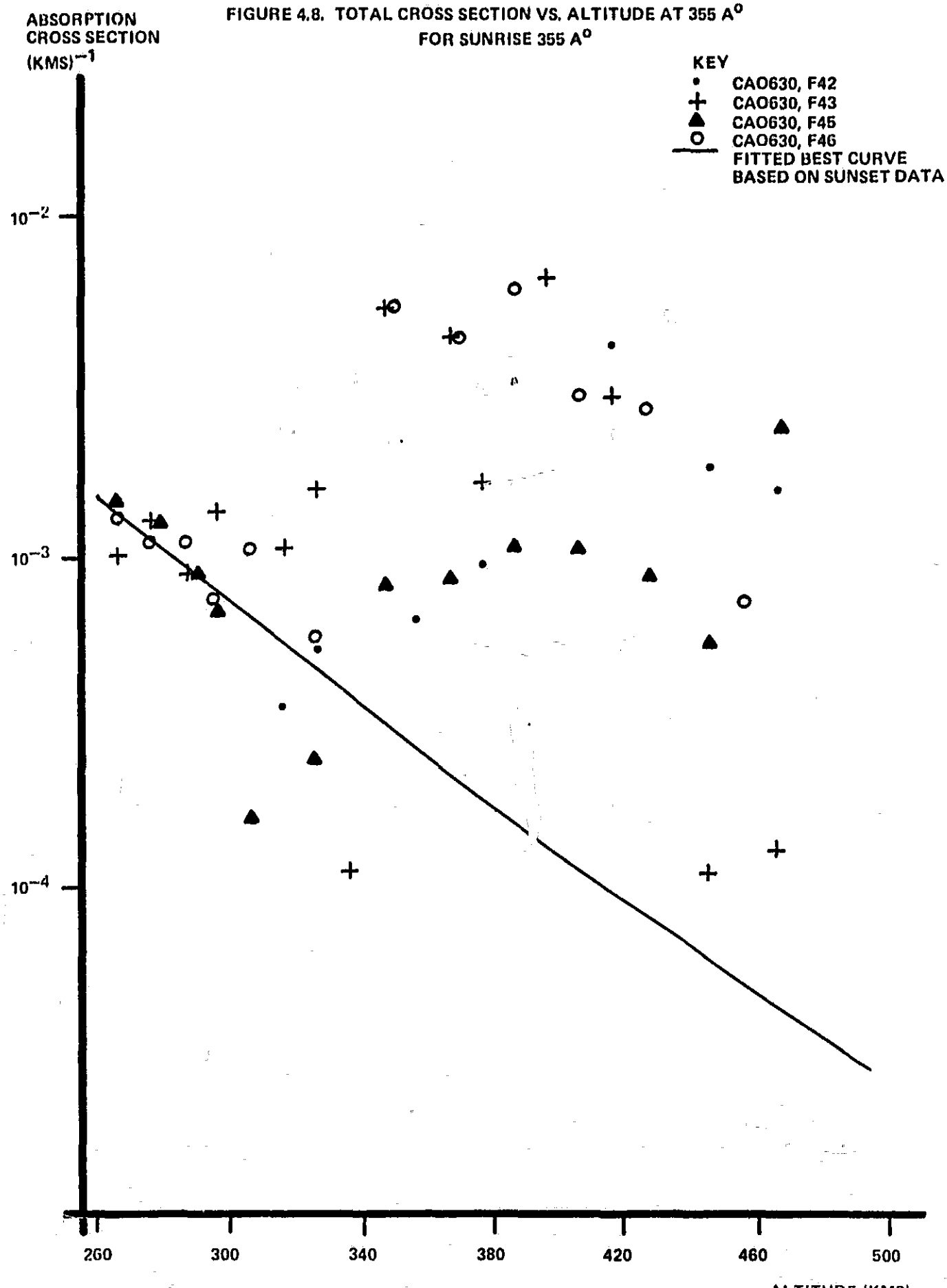

FIGURE 4.9. JACCHIA MODEL AT VARIOUS EXOSPHERIC TEMPERATURES OF O DENSITY VS. ALTITUDE

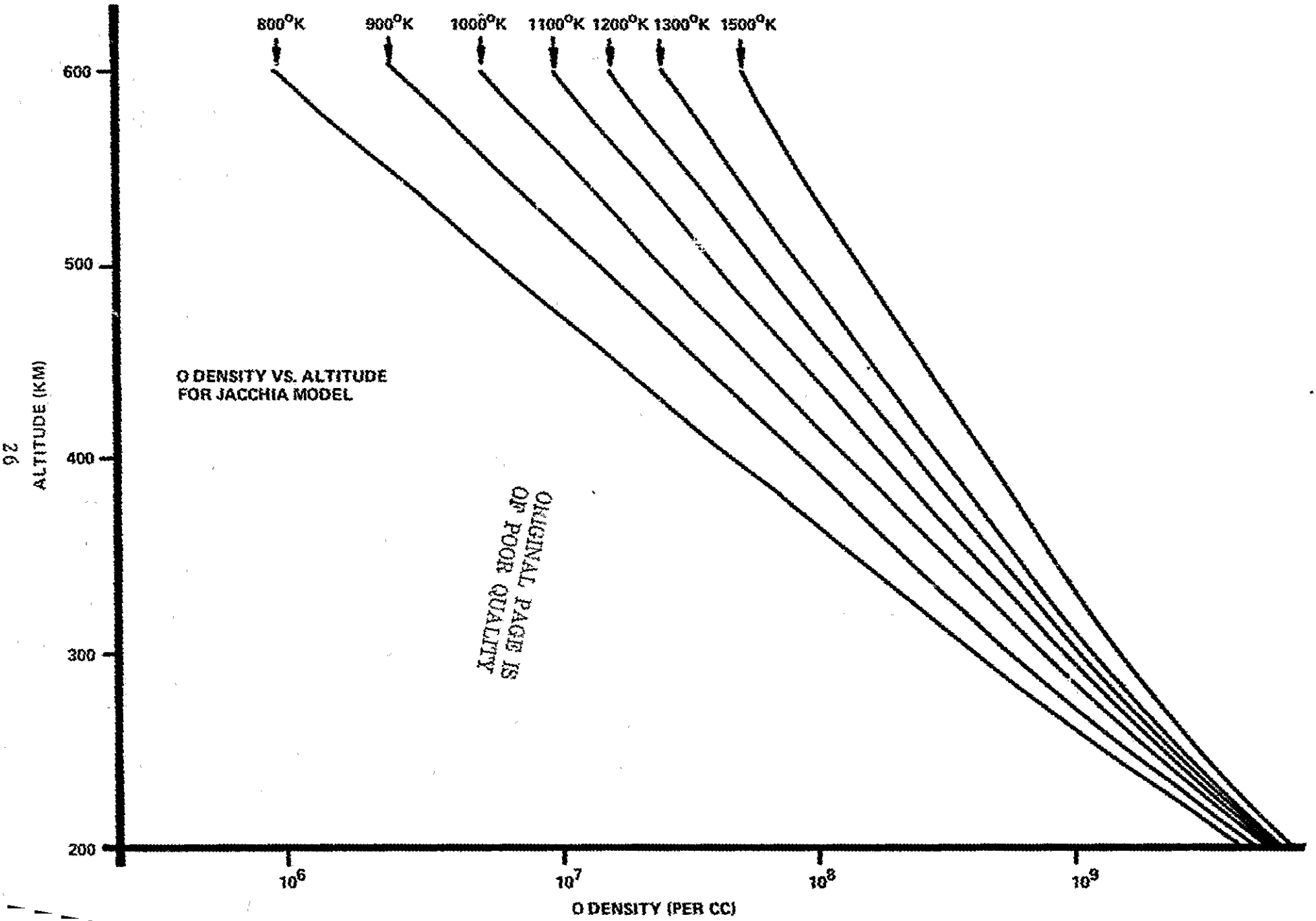

FIGURE 4.10. JACCHIA MODEL FOR VARIOUS EXOSPHERIC TEMPERATURE OF N_2 DENSITY VS. ALTITUDE

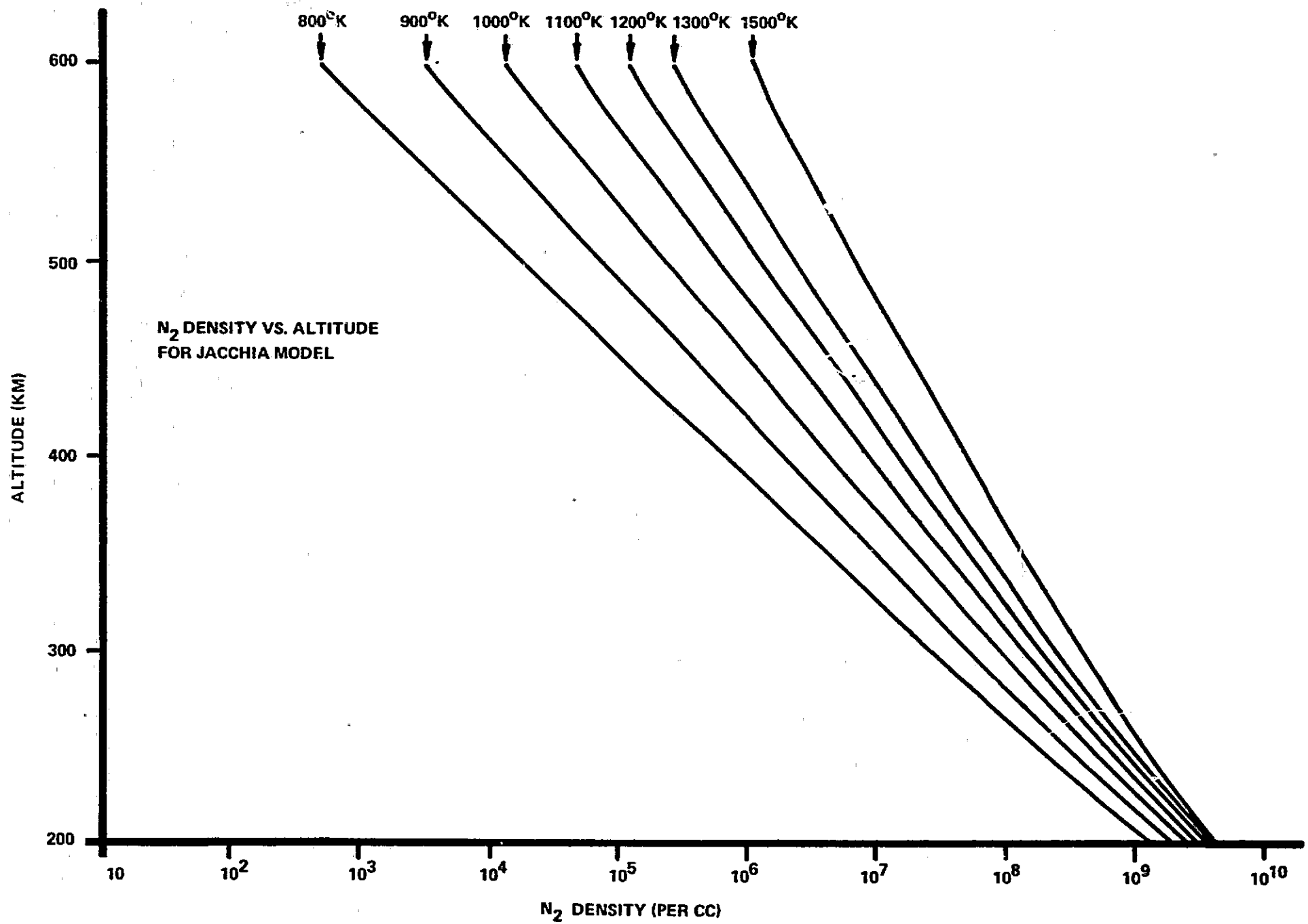

In Figures 4.9 and 4.10 we present the oxygen and molecular nitrogen densities versus altitude for different exospheric temperatures of the Jacchia (1971) model that was employed in our study. These graphs illustrate that a significant change in the density and, therefore, the attenuation characteristics of the atmosphere can be expected with changing exospheric temperature. O becomes more predominant with increasing altitude, so information about N_2 must be obtained from attenuation through the lower layers.

SECTION 5.0
DISCUSSION

We have in this project arrived at the goal which is to derive the N_2, O densities as a function of altitude from 260 km. to 500 km. above the surface of the Earth. However, the data obtained at sunrise is very erratic and showed no trend whatsoever thus giving us only sunset data to deal with. However, the sunset data was adequate to derive the absolute cross-sections at 285 Å and 355 Å of O and N_2 which is an unexpected by-product.

There are a number of possible explanations for the erratic data at sunrise. The sunrise data span was much longer in duration than the sunset portion and therefore promises much more information about the atmosphere. It is likely that our description of the atmosphere as varying only in the vertical direction is not valid and that variations in exospheric temperature around the globe become important. There is ample data to justify an extensive survey of this problem but we were unable to study this problem in depth within the time and funding constraints of the project. It is highly desirable to look at attenuation data in this region from other spacecraft. This combining of all the data available from many spacecraft will lead to a high accuracy density profiles and atmospheric model validation.

We thank NASA Headquarters for giving us an opportunity to participate in this program. We, in consultation with the Principal Investigator and the Technical Officer, propose to publish this work in a scientific journal at a later date.

Table I. Densities of Molecular Nitrogen and Atomic Oxygen From the Best Fitted Jacchia Model

NO.	ALTITUDE	DENSITY/CM^3	
		MOL. NITROGEN	OXYGEN
1	260	3.591×10^{8}	1.676×10^{9}
2	300	1.048×10^{8}	8.204×10^{8}
3	340	3.2×10^{7}	4.153×10^{8}
4	380	1.02×10^{7}	2.146×10^{8}
5	420	3.28×10^{6}	1.125×10^{8}
6	460	1.08×10^{6}	5.95×10^{7}
7	500	3.61×10^{5}	3.18×10^{7}

Table II. Cross-sections of N_2 and O at 285 Å and 355 Å

CONSTITUENT	CROSS-SECTIONS 285 Å	355 Å
MOL. NITROGEN	6.869±3.0	4.837±3.9
OXYGEN	6.282±0.6	7.612±0.8

UNIT = Megabarn = 10^{-18} cm^2

REFERENCES

1969 Hinteregger, H.E., and Hall, L.A., "Thermospheric Densities and Temperatures from EUV Absorption Measurements by OSO III," Space Research, 9, 519-529.

1971 Jacchia, L.G., "Revised Static Models of the Thermosphere and Exosphere With Emperical Temperature Profiles," S.A.O. Special Report 332.

1973 Knight, D.E., Uribe, R. and Woodgate, B.E., "Low Latitude Density Variations in the Atmosphere Between 200 and 400 km, from August 1969 to May 1970," Planet. Space. Sci., 21, 253-271.